applied optics

Leveraging statistical-spectral correlations of random metasurfaces for steganography and multi-wavelength cryptography

Romil Audhkhasi,[1] Maksym Zhelyeznyakov,[1] Steven Brunton,[2] and Arka Majumdar[1,3,*]

[1]Department of Electrical and Computer Engineering, University of Washington, Seattle, Washington 98195, USA
[2]Department of Mechanical Engineering, University of Washington, Seattle, Washington 98195, USA
[3]Department of Physics, University of Washington, Seattle, Washington 98195, USA
*arka@uw.edu

Received 14 March 2024; revised 16 April 2024; accepted 16 April 2024; posted 17 April 2024; published 9 May 2024

The ability to tailor the spectral response of photonic devices is paramount to the advancement of a broad range of applications. The vast design space offered by disordered optical media provides enhanced functionality for spectral tailoring while also making it challenging to map the spectral properties of such complex systems to their structural attributes. In this work, we investigate correlations between the configuration statistics of random metasurfaces and their spectral transmissivity in the visible, and leverage those to develop a reduced phase space. In the latter part of the manuscript, we use this reduced phase space to design a pixelated color filter that hides visual data within a preselected cover image for steganography. Furthermore, we design a pair of color filters that can collectively encrypt a given grayscale image in their spectral transmissivities. We envision such devices to create opportunities for the development of compact, next-generation cryptographic systems. More broadly, the results presented in this manuscript provide new, to the best of our knowledge, avenues for optimizing large-scale random metasurfaces to achieve enhanced optical functionalities for a wide variety of applications.

https://doi.org/10.1364/AO.523914

1. INTRODUCTION

Nature is abundant with randomness and disorder [1–5], and random media play a critical role in sustaining the environment around us [6,7]. Historically, ordered and periodic photonic structures have received considerable attention from the scientific community [8], and randomness and disorder have often been viewed as undesirable. Recently, owing to the wide range of functionalities exhibited by disordered systems found in nature, researchers have started investigating their optical properties. By judiciously exploiting the extent of randomness in such systems, several studies have proposed disordered photonic devices for applications in spectroscopy [9,10], imaging, and lasing [11].

The benefit of having a large design space in disordered photonic devices comes with the challenge of mapping their structural degrees of freedom to their optical response. Therefore, it is of immense importance to determine a tractable set of parameters that can be used to characterize and predict the optical properties of such complex systems. In this work, we investigate the correlation between the statistics governing the configuration of a random metasurface and its spectral transmissivity in the visible wavelength range. We consider metasurfaces consisting of a finite, two-dimensional array of Si nanopillars with their widths sampled from a normal distribution, placed on a SiO_2 substrate. We begin by analyzing the spectral responses of random metasurfaces generated from a specific normal distribution but having different sets of nanopillar widths and numbers of constituent nanopillars. Guided by the results of this analysis, we develop a reduced design space that maps the parameters of the normal distribution underlying our metasurfaces and the statistical properties of their transmission spectra.

In the latter part of the manuscript, we use our reduced phase space to design metasurfaces for steganography and multi-wavelength cryptography. In recent years, metasurfaces have been widely investigated for applications in data storage [12–27] and image encryption [28–33] due to their ability to manipulate light in the spatial and spectral domain. Here we use our random metasurfaces to design pixelated color filters that can hide image information within a chosen cover image for steganography. Furthermore, we design a pair of color filters that collectively encrypt the data of a given grayscale image into their respective wavelength-dependent spectral responses. We envision such compact data storage devices to lay the foundation of next-generation cryptographic and anti-counterfeiting systems.

The results presented in this manuscript will serve as a stepping stone for understanding optical phenomena in random photonic devices. The ability to leverage the strong correlations between the configuration statistics of random metasurfaces and their spectral responses could potentially pave the way for compact and highly efficient photonic devices for a broad range of applications.

2. RESULTS AND DISCUSSION

We begin by describing the design of our random metasurfaces followed by a study of the correlation between their configuration statistics and spectral transmissivity in Subsection 2.A. In Subsection 2.B, we leverage these correlations to design metasurfaces for steganography and multi-wavelength cryptography.

A. Correlation between the Configuration Statistics and Spectral Properties of a Random Metasurface

We consider random metasurfaces consisting of a two-dimensional array of Si nanopillars on a 1 μm thick SiO_2 substrate (Fig. 1). The array consists of $N \times N$ Si nanopillars placed on a square grid with a center-to-center separation of 500 nm. The nanopillars have a height of 500 nm, while their top and bottom faces are shaped like a square with side lengths sampled from a normal distribution. For convenience, we will refer to this structure as an $N \times N$ random metasurface hereon.

We wish to understand the correlation between the configuration statistics of our random metasurfaces and their spectral properties. The configuration statistics of a given random metasurface are governed by a normal distribution from which the side lengths L of its nanopillars are sampled. As an example, let us consider a 10×10 random metasurface constructed from a normal distribution with mean $\mu = 200$ nm and standard deviation $\sigma = 30$ nm. Figure 2(a) shows the probability density function (PDF) of the distribution. The PDF is normalized such that its integral over the entire range of L values is equal to unity.

We first use this PDF to construct 10 *instantiations* of the random metasurface. Here an instantiation refers to a specific selection of nanopillar side lengths from a given PDF. We calculate the wavelength-dependent transmissivity of each instantiation by conducting electromagnetic simulations in Lumerical finite difference time domain (FDTD). The simulation domain consists of perfectly matched layer (PML) boundary conditions on all sides and is defined such that the nanopillar array only occupies 80% of its total area in the x-y plane. The structure is illuminated by a normally incident plane wave from the top and transmissivity as a function of the wavelength is recorded by using a power flux monitor at the bottom.

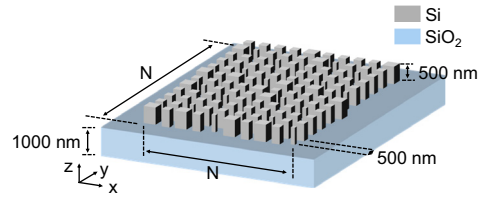

Fig. 1. Schematic of an $N \times N$ random metasurface.

Figure 2(b) shows the simulated wavelength-dependent transmissivity, T of the instantiations. The solid black line represents the mean transmission spectrum, while the blue band indicates the range of transmissivity values of the 10 instantiations at each wavelength. We observe that the range of transmissivity values at each wavelength is much smaller than the mean, indicating that the spectral response of a random metasurface is dictated by the PDF from which it is generated and not by its specific instantiation.

Next, we compare the spectral responses of random metasurfaces generated from the PDF shown in Fig. 2(a) but having a different number of nanopillars. Figure 2(c) shows the simulated transmission spectra of three random metasurfaces with $N = 10$, 15, and 20. To account for a change in the simulation domain area with increase in N, we multiply the spectra for $N = 15$ and 20 with the ratio of the mean transmittance of a bare substrate for the $N = 10$ case and that for the $N = 15$ and 20 cases, respectively. We observe that the spectral responses of all three metasurfaces possess a similar lineshape. This indicates that the spectral response of random metasurfaces sampled from the same PDF is independent of the number of their constituent nanopillars.

As mentioned above, a major challenge while designing random metasurfaces for various applications is the large design phase space associated with such devices. The strong correlations between the configuration statistics of random metasurfaces and their spectral properties allow for a reduction in the size of this phase space. To demonstrate this, we first define the spectral mean (mean(T)) and spectral variance (var(T)) associated with the transmission spectrum of a given metasurface as follows:

$$\text{mean(T)} = \frac{\int_{\lambda_1}^{\lambda_2} d\lambda T(\lambda)}{\int_{\lambda_1}^{\lambda_2} d\lambda}, \tag{1}$$

$$\text{var(T)} = \frac{\int_{\lambda_1}^{\lambda_2} d\lambda (T(\lambda) - \text{mean(T)})^2}{\int_{\lambda_1}^{\lambda_2} d\lambda}. \tag{2}$$

Here $T(\lambda)$ is the transmission spectrum of the random metasurface, and the integral is performed from $\lambda_1 = 400$ nm to $\lambda_2 = 800$ nm.

Figure 3 presents the dependence of the mean(T) and var(T) of a 10×10 random metasurface on the parameters μ and σ of its underlying normal distribution. To generate these plots, we first generate 63 random metasurfaces corresponding to nine μ values between 130 and 150 nm and seven σ values between 0 and 30 nm. These random metasurfaces are subsequently simulated, and their corresponding mean(T) and var(T) are interpolated over a finer, 241×31 grid of μ and σ values. It can be observed that the mean(T) is nearly independent of σ and reduces with an increase in μ. On the other hand, var(T) is influenced by both μ and σ. We note that, qualitatively, the mean(T) and var(T) of a random metasurface can be controlled nearly independently of each other by tuning its underlying normal distribution. This allows us to conveniently parameterize the phase space by using μ and σ instead of the widths of all the nanopillars constituting the metasurface.

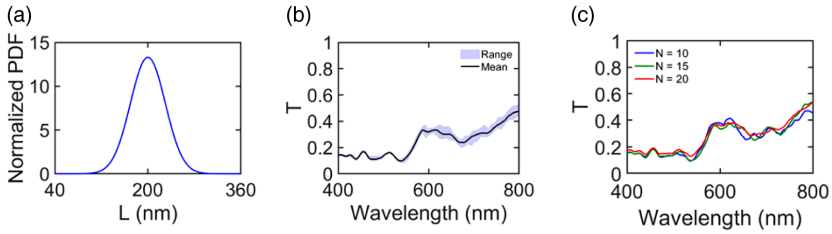

Fig. 2. (a) Probability density function of a normal distribution with $\mu = 200$ nm and $\sigma = 30$ nm. The PDF is normalized such that the total area under the curve is unity. (b) Transmission spectra of 10 instantiations of a random metasurface with nanopillar widths sampled from the PDF shown in part (a). The mean transmission spectrum is shown by the solid black line, and the range is shown by the shaded blue region around it. (c) Transmission spectra for three different random metasurfaces with $N = 10$, 15, and 20.

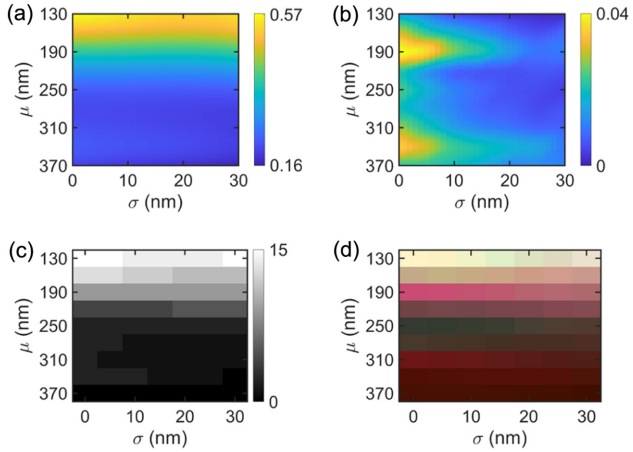

Fig. 3. (a) Mean(T), and (b) var(T) as a function of the normal distribution parameters μ and σ. (c) and (d) show the binned grayscale intensity map and RGB map, respectively, for metasurfaces on the non-interpolated 9×7 grid of μ and σ values.

In the next subsection, we use our reduced phase space to design metasurfaces for steganography and multi-wavelength cryptography.

B. Designing Random Metasurfaces for Steganography and Multi-Wavelength Cryptography

The ability to tailor the spectral means and variances of random metasurfaces can be leveraged to design color filters with predefined wavelength-averaged transmission properties. As an example, consider a random metasurface illuminated by a broadband visible light source and imaged in the near-field by using both an RGB sensor and a monochrome sensor. The RGB sensor will record three intensity values dependent on the overlap of the metasurface's spectral transmissivity with the red, green and blue sensor response curves. On the other hand, the monochrome sensor will record a single value proportional to the spectrally averaged transmissivity of the metasurface. In other words, while the grayscale value of the metasurface will be governed only by its spectral mean, its RGB value will depend on both its spectral mean and variance. Below we exploit this fact to design pixelated transmission filters for steganography and multi-wavelength cryptography.

We begin by calculating the near-field grayscale and RGB intensity maps of random metasurfaces generated from the non-interpolated 9×7 grid of μ and σ values [Figs. 3(c) and 3(d), respectively]. The grayscale values (ranging from 0 to 15) are calculated by integrating the transmissivity of each metasurface over the 400–800 nm wavelength range and binning the resulting set of values into 16 levels between the lowest and highest. Each value of the RGB triplet of a given metasurface is calculated using the following equation:

$$v_k = \left\lceil 256 \frac{\int_{\lambda_1}^{\lambda_2} d\lambda T_{\text{pixel}}(\lambda) T_k(\lambda)}{\int_{\lambda_1}^{\lambda_2} d\lambda T_k^2(\lambda)} \right\rceil. \quad (3)$$

Here $T_{\text{pixel}}(\lambda)$ and $T_k(\lambda)$ ($k = R$, G, or B) are the transmission spectra of the metasurface and the filter response of the sensor, respectively. For simplicity, we assume the filter responses of the R, G, and B sensors to be Lorentzian with amplitude 1, full width at half-maximum 50 nm, and centered at wavelengths of 630, 532 and 465 nm, respectively. The integral is performed from $\lambda_1 = 400$ nm to $\lambda_2 = 800$ nm, and $\lceil x \rceil$ denotes the greatest integer less than or equal to x.

We use the set of 9×7 random metasurfaces to design a pixelated transmission filter that hides data within a preselected cover image. This is referred to as steganography. The hidden data are completely invisible to the naked eye and can only be recovered when the filter is illuminated by a broadband source and imaged in the near-field using a monochrome sensor. For simplicity, we use as our cover image a 6×7 binary image of the letter "W" made up of the colors peach and pink with RGB values (230, 175, 160) and (226, 136, 150), respectively. The hidden data are a two-dimensional array of integers 1, 2, and 3.

The filter is designed as a 42×49 grid of pixels, where each pixel is a 10×10 random metasurface. Each 7×7 block of filter pixels encodes a single pixel of the cover image in its RGB response and a 7×7 image of a digit in its grayscale response [Fig. 4(a)]. For encoding the peach-colored pixels of the cover image, we choose from two types of random metasurfaces that have RGB values closest to (230, 175, 160) but different grayscale values of either 11 or 12. The same procedure is repeated for encoding the pink pixels of the cover image by using random metasurfaces with RGB values closest to (226, 136, 150) but having grayscale levels of either 10 or 11. Figures 4(b) and 4(c) show the near-field RGB and grayscale images of the pixelated filter. One can observe that the filter displays an image of the letter "W" in its RGB image while revealing a hidden sequence of numbers in its grayscale image. We envision such a device to be useful for anti-counterfeiting applications, where

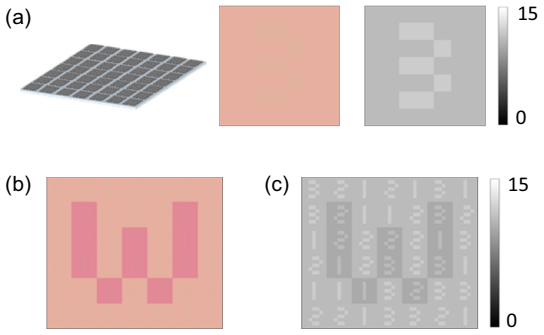

Fig. 4. (a) Left panel shows a schematic of a block of 7 × 7 filter pixels. The corresponding RGB and grayscale images are shown in the middle and the right panels, respectively. (b) Near-field RGB and (c) near-field grayscale image of the full pixelated filter.

the hidden image (in this case, the sequence of numbers) serves as an authentication key.

Next, we consider the design of pixelated transmission filters capable of encrypting 4-bit grayscale images in their spectral response. A 4-bit grayscale image has 16 intensity levels, with pixel intensity values ranging from 0 to 15. Here we wish to design a pair of filters that collectively encrypt a 100 × 100 pixel, 4-bit grayscale image of the letter "W," known as the plain image (left panel of Fig. 5). The encryption process begins by generating two seemingly random images (image 1 and 2) such that a pixel-wise XOR operation between them results in the plain image. These images are subsequently encoded on two separate filters. The division of plain image data into two sets of random images ensures that a recipient in possession of only one of the two filters cannot recover any meaningful information about the plain image.

We model the two filters as 100 × 100 pixel square grids, where each pixel is a 10 × 10 random metasurface chosen from the phase space shown in Figs. 3(a) and 3(b). The first step of the filter design process is the truncation of the 241 × 31 phase space by selecting random metasurfaces having spectral means close to 16 equally spaced levels between 0.16 and 0.57. Next, we randomly select four metasurfaces corresponding to each level so as to give a final set of 16 × 4 metasurfaces. We calculate two matrices for this set of metasurfaces. The first matrix, G (top middle panel of Fig. 5), contains the grayscale intensity values of all the metasurfaces, binned into 16 levels from 0 to 15. The second matrix, X (bottom middle panel of Fig. 5), is obtained by binning mean(T) and var(T) for the chosen set of metasurfaces into 16 levels and performing an XOR operation between them.

Figure 5 describes the process of selecting pixels of the two filters from the set of 16 × 4 random metasurfaces. For image 1, the grayscale value of each pixel is used to randomly select a metasurface belonging to the same grayscale level from matrix G (highlighted by a blue box in Fig. 5). The selected metasurface is assigned to filter 1 at the same location as the considered pixel from image 1. The same process is repeated for each pixel in image 2, where pixels are now selected from matrix X and assigned to filter 2. The right panel of Fig. 5 shows a map of μ and σ values for the normal distributions governing the pixels of the two generated filters. We observe that these look completely random and do not reveal any meaningful information about the plain image.

To perform decryption, we calculate the transmission spectra of the set of 16 × 4 filters using FDTD simulations. This gives us the pixel-wise wavelength-dependent transmissivity of filters 1 and 2. Figures 6(a) and 6(b) show the RGB and grayscale near-field images of the two filters calculated based on their respective transmission spectra. It can be observed that either the RGB or the grayscale near-field images of both filters alone do not reveal any meaningful information about the plan image.

Next, we calculate the binned mean(T) and var(T) of the pixels of filter 2 [left panel of Fig. 6(c)] based on their simulated transmission spectra. Taking a pixel-wise XOR between these gives us image 2 which, upon the application of an XOR operation with the binned grayscale profile of filter 1 (image 1), reveals the encrypted image of the letter "W." We observe that the output image, while having a high level of similarity to the plain image, possesses significantly more noise. This can be attributed to slight differences between the simulated and interpolated mean(T) and var(T) values of the metasurfaces that get magnified after binning into 16 levels. This issue can be rectified by using the simulated spectral responses of the 16 × 4 metasurfaces to construct the matrices G and X during encryption. The output image in this case (not shown in Fig. 6 but verified through separate calculations) matches exactly with the plain image.

Finally, we provide a qualitative assessment of the security provided by our encryption scheme. For this purpose, let us assume our encryption system to be a black box that accepts a 4-bit grayscale image (plain image) at its input and generates a pair of transmission filters (ciphers) at the output. As a first step, our encryption scheme requires the plain image to be divided into two intermediate images that are related to it via an XOR operation. This ensures that, for every pixel of the plain image, there exist multiple possible pixel value pairs for the intermediate images. Additionally, for every pixel of each of the two intermediate images, there exist multiple metasurfaces that satisfy the corresponding selection criteria. These two attributes of our encryption scheme ensure that, for a given plain image, the encryption black box produces one of several possible filter pairs. We note that several common cryptographic attacks such as the chosen plaintext attack (CPA) and known plaintext attack (KPA) rely on exploiting the plaintext-cipher relationship to break the encryption system. The one-to-many mapping between the plain image and ciphers for our encryption system makes it extremely robust to such attacks.

3. CONCLUSION

In this work, we investigated correlations between the configuration statistics of random metasurfaces and their spectral transmissivity in the visible wavelength range. We considered metasurfaces consisting of Si nanopillars with widths sampled from a normal distribution, placed on a SiO_2 substrate. We showed that the spectral lineshapes of metasurfaces generated from the same normal distribution are independent of the exact values of their nanopillar widths or the number of their constituent nanopillars. Furthermore, we developed a mapping between the parameters of the normal distribution underlying our random metasurfaces and their spectral mean and variance.

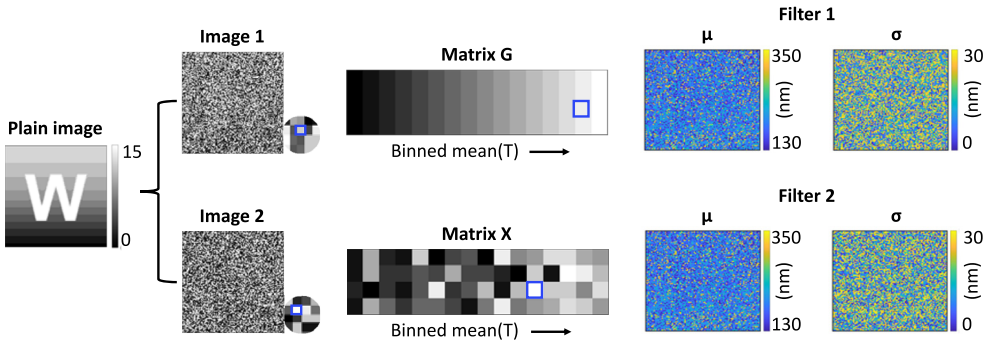

Fig. 5. Encryption of a 4-bit, 100 × 100 pixel grayscale image of the letter "W" on two transmission filters. The image is first split into images 1 and 2, which are subsequently encoded on filters 1 and 2, respectively. The middle panel explains the pixel selection process for the two filters for specific pixels of images 1 and 2 (shown by the highlighted blue boxes in the image insets).

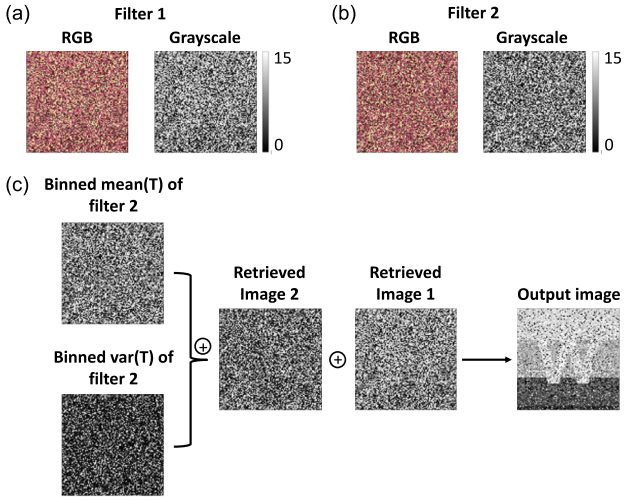

Fig. 6. Near-field RGB and grayscale images of (a) filter 1 and (b) filter 2. (c) Decryption process for retrieving the plain image.

In the latter part of the manuscript, we leveraged the reduced phase space resulting from this analysis to design pixelated transmission filters for steganography and multi-wavelength cryptography in the visible. By exploiting the ability to independently modulate the spectral mean and variance of our metasurfaces, we designed a pixelated filter that hides a sequence of digits within a preselected cover image. The encoded data are invisible to the naked eye and can only be recovered from the near-field grayscale image of the filter. We further exploited the design flexibility afforded by our reduced phase space to design a pair of transmission filters for encrypting a 4-bit grayscale image. The random structural configuration and near-field optical response of either of the two filters make it extremely challenging for an adversary to retrieve the hidden image without having access to the other.

We note that, while the current work considered random metasurfaces sampled from a normal distribution, the analysis presented herein can potentially be extended to a broader class of probability density functions. Furthermore, while this study focused on wavelength-averaged optical properties of random metasurfaces, future work may investigate strategies to predict their full spectral response from their configuration statistics. The ability to design random metasurfaces with tailored spectral responses will be useful for a wide range of applications. For instance, in the context of optical cryptography, metasurfaces with predefined transmission spectra can be used for preferentially dispersing encrypted data across a set of preselected wavelengths. This set of wavelengths can subsequently be used as a decryption key, thus adding an additional layer of security to the decryption process.

Despite the above limitations, the results presented in this manuscript provide new avenues for optimizing large-scale random metasurfaces to achieve enhanced optical functionalities for a broad class of applications.

Funding. Defense Advanced Research Projects Agency (HR001123C0034).

Disclosures. The authors declare no conflicts of interest.

Data availability. Data underlying the results presented in this paper are not publicly available at this time but may be obtained from the authors upon reasonable request.

REFERENCES

1. S. Berthier, E. Charrion, and J. Boulenguez, "Morphological structure and optical properties of the wings of Morphidae," Insect Sci. **13**, 145–158 (2006).
2. J. Sun, B. Bhushan, and J. Tonga, "Structural coloration in nature," RSC Adv. **3**, 14862–14889 (2013).
3. S. Kinoshita, S. Yoshioka, and K. Kawagoe, "Mechanisms of structural colour in the Morpho butterfly: cooperation of regularity and irregularity in an iridescent scale," Proc. R. Soc. London Ser. B **269**, 1417–1421 (2002).
4. S. Tadepalli, J. M. Slocik, M. K. Gupta, *et al.*, "Bio-optics and bio-inspired optical materials," Chem. Rev. **117**, 12705–12763 (2017).
5. P. Vukusic, B. Hallam, and J. Noyes, "Brilliant whiteness in ultrathin beetle scales," Science **315**, 348 (2007).
6. M. Rothammer, C. Zollfrank, K. Busch, *et al.*, "Tailored disorder in photonics: learning from nature," Adv. Opt. Mater. **9**, 2100787 (2021).
7. D. S. Wiersma, "Disordered photonics," Nat. Photonics **7**, 188–196 (2013).
8. J. D. Joannopoulos, P. R. Villeneuve, and S. Fan, "Photonic crystals," Solid State Commun. **102**, 165–173 (1997).
9. B. Redding, S. F. Liew, R. Sarma, *et al.*, "Compact spectrometer based on a disordered photonic chip," Nat. Photonics **7**, 746–751 (2013).
10. Z. Xu, Z. Wang, M. E. Sullivan, *et al.*, "Multimodal multiplex spectroscopy using photonic crystals," Opt. Express **11**, 2126–2133 (2003).
11. H. Cao, "Lasing in random media," Waves Random Media **13**, R1–R39 (2003).

12. W. Ye, F. Zeuren, X. Li, *et al.*, "Spin and wavelength multiplexed nonlinear metasurface holography," Nat. Commun. **7**, 11930 (2016).
13. F. Walter, G. Li, C. Meier, *et al.*, "Ultrathin nonlinear metasurface for optical image encoding," Nano Lett. **17**, 3171–3175 (2017).
14. P. Yu, J. Li, S. Zhang, *et al.*, "Dynamic Janus metasurfaces in the visible spectral region," Nano Lett. **18**, 4584–4589 (2018).
15. K. T. P. Lim, H. Liu, Y. Liu, *et al.*, "Holographic colour prints for enhanced optical security by combined phase and amplitude control," Nat. Commun. **10**, 25 (2019).
16. Y. Tang, Y. Intaravanne, J. Deng, *et al.*, "Nonlinear vectorial metasurface for optical encryption," Phys. Rev. Appl. **12**, 024028 (2019).
17. X. Luo, Y. Hu, X. Li, *et al.*, "Integrated metasurfaces with microprints and helicity-multiplexed holograms for real-time optical encryption," Adv. Opt. Mater. **8**, 1902020 (2020).
18. P. Zheng, Q. Dai, Z. Li, *et al.*, "Metasurface-based key for computational image encryption," Sci. Adv. **7**, eabg0363 (2021).
19. Z. Xu, H. Luo, H. Zhu, *et al.*, "Nonvolatile optically reconfigurable radiative metasurface with visible tunability for anticounterfeiting," Nano Lett. **21**, 5269–5276 (2021).
20. C. Choi, S.-E. Mun, J. Sung, *et al.*, "Hybrid state engineering of phase-change metasurface for all-optical cryptography," Adv. Funct. Mater. **31**, 2007210 (2021).
21. S. Du, Z. Liu, C. Sun, *et al.*, "Cross-nanofin-based waveplate pixels for broadband hybrid polarization coding in near-field," Nanophotonics **10**, 1505–1515 (2021).
22. T. Liu, W. Li, Y. Meng, *et al.*, "High-fidelity multiplexing meta-hologram for information display, storage and encryption," Mater. Des. **224**, 111353 (2022).
23. M. Q. Mehmood, J. Seong, M. Ashar Naveed, *et al.*, "Single-cell-driven tri-channel encryption meta-displays," Adv. Sci. **9**, 2203962 (2022).
24. H. L. Wang, H. F. Ma, and T. J. Cui, "A polarization-modulated information metasurface for encryption wireless communications," Adv. Sci. **9**, 2204333 (2022).
25. I. Kim, J. Jang, G. Kim, *et al.*, "Pixelated bifunctional metasurface-driven dynamic vectorial holographic color prints for photonic security platform," Nat. Commun. **12**, 3614 (2021).
26. K. Li, J. Wang, W. Cai, *et al.*, "Electrically switchable, polarization-sensitive encryption based on aluminum nanoaperture arrays integrated with polymer-dispersed liquid crystals," Nano Lett. **21**, 7183–7190 (2021).
27. Y. Cao, L. Tang, J. Li, *et al.*, "Four-channel display and encryption by near-field reflection on nanoprinting metasurface," Nanophotonics **11**, 3365–3373 (2022).
28. G. Qu, W. Yang, Q. Song, *et al.*, "Reprogrammable meta-hologram for optical encryption," Nat. Commun. **11**, 5484 (2020).
29. Z. Li, M. Premaratne, and W. Zhu, "Advanced encryption method realized by secret shared phase encoding scheme using a multi-wavelength metasurface," Nanophotonics **9**, 3687–3696 (2020).
30. J. Li, Z. Guan, H.-C. Liu, *et al.*, "Metasurface-assisted indirect-observation cryptographic system," Laser Photonics Rev. **17**, 2200342 (2022).
31. R. Audhkhasi and M. L. Povinelli, "Generalized multi-channel scheme for secure image encryption," Sci. Rep. **11**, 22669 (2021).
32. R. Audhkhasi, M. R. Lien, and M. L. Povinelli, "Experimental implementation of metasurfaces for secure multi-channel image encryption in the infrared," Adv. Opt. Mater. **11**, 2203155 (2023).
33. R. Audhkhasi and M. L. Povinelli, "Full spectral image encryption in the infrared using an electrically reconfigurable metasurface and a matched detector," Adv. Photonics Res. **5**, 2300254 (2024).